

Experimental Confirmation of Different Mechanisms of Evaporation from Ink-Bottle Type Pores: Equilibrium, Pore Blocking, and Cavitation

Peter I. Ravikovitch and Alexander V. Neimark*

The Center for Modeling and Characterization of Nanoporous Materials, TRI/Princeton,
601 Prospect Avenue, Princeton, New Jersey 08540-0625

Received June 27, 2002. In Final Form: September 24, 2002

We present a new classification of physical mechanisms of adsorption hysteresis in ink-bottle type pores confirmed by experimental studies of capillary condensation of N₂, Ar, and Kr at 77.4 and 87.4 K in ordered 3D cage-like structures of FDU-1 and SBA-16 nanoporous templated silicas with narrow pore size distribution. An analysis of the hysteresis loops and scanning desorption isotherms on FDU-1 with ~15 nm spherical pores reveals three mechanisms of evaporation: (1) evaporation from the blocked cavities controlled by the size of connecting pores (classical ink-bottle or pore blocking effect); (2) spontaneous evaporation caused by cavitation of the stretched metastable liquid; and, for the first time, (3) near-equilibrium evaporation in the region of hysteresis from unblocked cavities that have access to the vapor phase. Studies of the temperature dependence of the hysteresis loop showed a transition between the cavitation and the pore blocking regimes of evaporation, which opens up the possibility to tune the experimental conditions in order to characterize the pore neck size distribution. A similar transition was also observed for Kr in SBA-16 silica with ~8.5 nm pores. The pressure of cavitation was found to depend on the pore geometry. This conclusion questions the conventional assumption that the pressure of cavitation, which determines the lower closure point of the hysteresis loop, is a unique function of the adsorbate and the temperature. The experimental results agree with the nonlocal density functional theory (NLDFT) of capillary condensation hysteresis in spherical cavities reported earlier (Ravikovitch, P. I.; Neimark, A. V. *Langmuir* 2002, 18, 1550).

1. Introduction

Following the classical works of Kraemer,¹ McBain,² and Cohan,³ the phenomenon of capillary hysteresis in pores of varying cross section and pore networks is usually explained by the pore blocking effect.^{4,5} The pore blocking effect is most pronounced in ink-bottle type pores, the simplest image of which is a spheroidal cavity fitted with a narrow cylindrical neck. A qualitative explanation of the capillary hysteresis in the ink-bottle pore is as follows. The pore filling in the process of condensation follows the formation of a liquid film on the cavity wall and thus is controlled by the radius of curvature of the cavity, r_c . The pressure of condensation p_c is given by the Kelvin–Laplace equation, $p_c/p_0 = \exp(-2\gamma v/RTr_c)$, where p_0 is the saturation vapor pressure at the given temperature T , γ is the liquid–vapor surface tension, v is the liquid molar volume, R is the universal gas constant. The evaporation in the process of desorption occurs after the formation of a hemispherical meniscus in the pore neck and thus is controlled by the radius of the neck, r_n . The pressure of desorption is determined by the Kelvin–Laplace equation for the equilibrium meniscus in the cylindrical neck $p_d/p_0 = \exp(-2\gamma v/RTr_n)$.

This concept has been elaborated later by Broekhoff and de Boer.⁶ Similarly to the mechanism of filling of

cylindrical pores,⁷ they associated the condition of condensation in the cavity with the achievement of the limit of stability of metastable adsorption films on the spherical wall. Broekhoff and de Boer used the Derjaguin principle of the additive action of capillary and surface forces⁸ to determine the condition of stability of adsorbed films and also the condition of equilibrium between the adsorbed film and the condensed liquid for cylindrical and spherical pores. The equations they derived for the pressure of spontaneous condensation and the pressure of equilibrium are referred to as the Derjaguin–Broekhoff–de Boer (DBdB) equations.⁶ For many years, the DBdB equations for the limit of stability of adsorption films on the spherical wall and for the equilibrium meniscus in the cylindrical neck represented the best quantitative description of the capillary condensation hysteresis in ink-bottle type pores.

The concept of pore blocking in ink-bottle type pores was successfully employed to describe the triangular hysteresis loops of type H2 by IUPAC classification typical for porous glasses.⁴ The pore structure of these materials is disordered and represents a network of channels with prominent enlargements and constrictions as shown by high-resolution microscopy and scattering data^{9a} and by an off-lattice reconstruction method.^{9b} Gelb and Gubbins¹⁰ mimicked this structure by molecular simulations of the process of formation of porous glasses. To account for networking effects, in the early 80s, Wall and Brown,^{11a}

* Corresponding author. E-mail: aneimark@triprinceton.org.

(1) Kraemer, E. O. *Treatise on Physical Chemistry*, Taylor, H. S., Ed.; Van Nostrand: New York, 1931; p 1661.

(2) McBain, J. W. *J. Am. Chem. Soc.* **1935**, *57*, 699.

(3) Cohan, L. H. *J. Am. Chem. Soc.* **1938**, *60*, 433.

(4) Everett, D. H. *The Solid–Gas Interface*; Flood, E. A., Ed.; Dekker: New York, 1967; Vol. 2.

(5) Gregg, S. J.; Sing, K. S. W. *Adsorption, Surface Area and Porosity*; Academic Press: New York, 1982.

(6) Broekhoff, J. C. P.; de Boer, J. H. *J. Catal.* **1968**, *10*, 153.

(7) Broekhoff, J. C. P.; de Boer, J. H. *J. Catal.* **1967**, *9*, 8.

(8) Derjaguin, B. V. *Acta Phys. Chem. URSS* **1940**, *12*, 181.

(9) (a) Levitz, P. E.; Ehret, G.; Sinha, S. K.; Drake, J. M. *J. Chem. Phys.* **1991**, *95*, 6151. (b) Pellenq, R.-J. M.; Rousseau, B.; Levitz, P. E. *Phys. Chem. Chem. Phys.* **2001**, *3*, 1207.

(10) Gelb, L. D.; Gubbins, K. E. *Langmuir* **1998**, *14*, 2097.

(11) (a) Wall, G. C.; Brown, R. J. C. *J. Colloid Interface Sci.* **1981**, *82*, 141. (b) Mason, G. J. *J. Colloid Interface Sci.* **1982**, *88*, 36.

Mason,^{11b} and Neimark¹² and later Seaton¹³ developed the percolation theory of capillary condensation and desorption in the network of cavities with multiple necks, assuming that the condensation in a cavity is controlled by its size while the desorption from a cavity is controlled by the smallest neck in a chain of necks connecting the cavity with the vapor phase. In particular, Neimark¹² showed that the behavior of scanning isotherm of Xe on porous glass⁴ follows the predictions of the percolation theory and developed a method for calculations of the neck size distribution.

Recently, the problem of adsorption hysteresis in ink-bottle type pores and the role of pore network connectivity attracted renewed attention.^{9b,14,15} Using molecular dynamics simulations Sarkisov and Monson^{15a} have questioned the existence of pore blocking effects in pores of simple geometry. Monte Carlo simulations of adsorption in model disordered systems have shown that pore blocking effects^{9b} and network connectivity¹⁴ have little influence on the shape of the hysteresis loop. Kierlik et al.¹⁶ and Woo et al.^{15b} developed lattice DFT models of sorption in disordered media and constructed, without invoking any networking effects, the hysteresis loops similar in shape to the experimental adsorption isotherms on porous glasses.

Advances in experimental investigations were related to the development of new nanoporous materials with an ordered structure of pores, most of which were synthesized using regular surfactant and micellar mesophases as templates.^{17–20} The pores in these materials resemble with the greatest accuracy the simple geometrical models of cylindrical channels¹⁷ or spherical cavities^{18–20} which can be investigated theoretically in great detail. That is, the ordered nanoporous materials provide a unique opportunity to compare theoretical predictions and experimental data without invoking adjustable parameters.

In the preceding paper,²¹ we developed a nonlocal density functional theory (NLDFT) model for capillary

(12) (a) Neimark, A. V. *Rep. Acad. Sci. USSR (Doklady Akademii Nauk SSSR)* **1983**, 273, 384. (b) Neimark, A. V. *Russian J. Phys. Chem. (Z. Fiz. Khim.)* **1986**, 60, 1745. (c) *Stud. Surf. Sci. Catal.* **1991**, 62, 67.

(13) Seaton, N. A. *Chem. Eng. Sci.* **1991**, 46, 1895.

(14) Gelb, L. D.; Gubbins, K. E. *Fundamentals of Adsorption* 7; Kaneko, K., Kanoh, H., Hanzawa, Y., Eds.; IK International: Chiba City, 2002; p 333.

(15) (a) Sarkisov, L. D.; Monson, P. A. *Langmuir* **2001**, 17, 7600. (b) Woo, H.-J.; Sarkisov, L. D.; Monson, P. A. *Langmuir* **2001**, 17, 7472.

(16) (a) Kierlik, E.; Rosinberg, M. L.; Tarjus, G.; Viot, P. *Phys. Chem. Chem. Phys.* **2001**, 3, 1201–1206. (b) Kierlik, E.; Monson, P. A.; Rosinberg, M. L.; Sarkisov, L.; Tarjus, G. *Phys. Rev. Lett.* **2001**, 87, 055701.

(17) (a) Kresge, C. T.; Leonowicz, M. E.; Roth, W. J.; Vartuli, J. C.; Beck, J. S. *Nature* **1992**, 359, 710. (b) Zhao, D. Y.; Feng, J. L.; Huo, Q. S.; Melosh, N.; Fredrickson, G. H.; Chmelka, B. F.; Stucky, G. D. *Science* **1998**, 279, 548. (c) Inagaki, S.; Guan, S.; Ohsuna, T.; Terasaki, O. *Nature* **2002**, 416, 34. (d) Van Der Voort, P.; Ravikovich, P. I.; De Jong, K. P.; Benjelloun, M.; Van Bavel, E.; Janssen, A. H.; Neimark, A. V.; Weckhuysen, B. M.; Vansant, E. F. *J. Phys. Chem. B* **2002**, 106, 5873.

(18) (a) Yu, C.; Yu, Y.; Zhao, D. *Chem. Commun.* **2000**, 575. (b) Yu, C.; Yu, Y.; Miao, L.; Zhao, D. *Microporous Mesoporous Mater.* **2001**, 44–45, 65. (c) Matos, J. R.; Mercuri, L. P.; Kruk, M.; Jaroniec, M. *Langmuir* **2002**, 18, 884. (d) Matos, J. R.; Kruk, M.; Mercuri, L. P.; Jaroniec, M.; Asefa, T.; Coombs, N.; Ozin, G. A.; Kamiyama, T.; Terasaki, O. *Chem. Mater.* **2002**, 14, 1903.

(19) (a) Guan, S.; Inagaki, S.; Ohsuna, T.; Terasaki, O. *J. Am. Chem. Soc.* **2000**, 122, 5660. (b) Sakamoto, Y.; Diaz, I.; Terasaki, O.; Zhao, D.; Pérez-Pariente, J.; Kim, J. M.; Stucky, G. D. *J. Phys. Chem. B* **2002**, 106, 3118. (c) Lukens, W. W.; Yang, P.; Stucky, G. D. *Chem. Mater.* **2001**, 13, 28. (d) Lukens, W. W.; Stucky, G. D. *Chem. Mater.* **2002**, 14, 1665. (e) Kim, J. M.; Stucky, G. D. *Chem. Commun.* **2000**, 1159.

(20) (a) Zhao, D. Y.; Huo, Q. S.; Feng, J. L.; Chmelka, B. F.; Stucky, G. D. *J. Am. Chem. Soc.* **1998**, 120, 6024. (b) Sakamoto, Y. H.; Kaneda, M.; Terasaki, O.; Zhao, D. Y.; Kim, J. M.; Stucky, G.; Shim, H. J.; Ryoo, R. *Nature* **2000**, 408, 449. (c) Van Der Voort, P.; Benjelloun, M.; Vansant, E. F. *J. Phys. Chem. B* **2002**, 106, 9027.

(21) Ravikovich, P. I.; Neimark, A. V. *Langmuir* **2002**, 18, 1550.

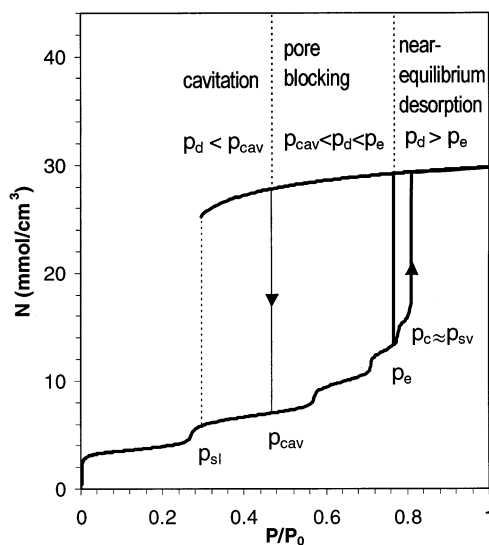


Figure 1. NLDFT N_2 adsorption–desorption isotherm at 77 K in 15.5 nm spherical cavity (thick solid line). The theoretical pressures of liquidlike spinodal, equilibrium, and vaporlike spinodal are denoted, respectively, as p_{sl} , p_e , and p_{sv} . Experimentally observed pressures of spontaneous capillary condensation and cavitation are denoted as p_c and p_{cav} , respectively ($p_c \approx p_{\text{sv}}$ and $p_{\text{sl}} < p_{\text{cav}} < p_e$). Three possible regimes of evaporation from the cavity are classified with respect to the pressure p_d of desorption from the neighboring pores or from the pore neck (see text in Discussion section).

condensation in spherical cavities. The theory allows us to construct stable and metastable equilibrium states, which possess a spherical symmetry compliant with the cavity geometry. The isotherm of these states forms a hysteresis loop comprising two branches, the adsorption branch of low density, or vaporlike states, and the desorption branch of high density, or liquidlike states (Figure 1). The pressure of the equilibrium transition p_e separates the stable and metastable states. At $p < p_e$, the adsorption branch corresponds to the stable adsorption films while the desorption branch corresponds to the metastable stretched liquid. The desorption branch terminates at the liquidlike spinodal, p_{sl} , the limit of mechanical stability of stretched condensed liquid. At $p > p_e$, the desorption branch corresponds to the stable condensed liquid while the adsorption branch corresponds to the metastable adsorption film. The adsorption branch terminates at the vaporlike spinodal, p_{sv} , which represents the limit of mechanical stability of the metastable adsorption film. In general, the pressures of condensation and desorption are controlled by the nucleation barriers at given experimental conditions²² and cannot be determined from the NLDFT calculations of thermodynamic equilibrium states. Thus, the theoretical spinodal pressures give the upper and lower bounds for the experimental hysteresis loop. A comparison of the theoretical results with the reference experiments allowed us to make several conclusions about the mechanisms of hysteresis in ink-bottle type pores.

The results of NLDFT calculations were found to be in quantitative agreement with experimental data on adsorption of nitrogen at 77.4 K in templated nanoporous silica with ordered structure of cage-like pores.²¹ In sufficiently large pores, which exhibit wide hysteresis loops, the condensation was shown to occur near the vaporlike spinodal, in accord with the classical scenario of spontaneous condensation (condensation pressure is

(22) Vishnyakov, A.; Neimark, A. V. *J. Phys. Chem. B* **2001**, 105, 7009.

denoted as p_c in Figure 1). In the further discussion, this condensation mechanism is referred to as the *near-spinodal condensation*. The NLDFT predictions for the equilibrium and vaporlike spinodal pressures asymptotically merge with the DBdB equations⁶ for cavity diameters exceeding ca. 10 nm. At the same time, we argued that there are two sorption mechanisms which are not accounted for in the DBdB theory.

First, the DBdB theory rules out the possibility of equilibrium capillary condensation and/or desorption in spherical cavities. We have shown that in sufficiently small cavities (for example for materials reported in refs 19a, 19b) the condensation occurs reversibly without a hysteresis and, most importantly, the pressure of condensation corresponds to the equilibrium pressure predicted by the NLDFT.²¹ With respect to sorption of nitrogen at 77.4 K, this mechanism of equilibrium condensation and desorption is expected in cavities with the diameter between ~ 3 and ~ 6 nm. In such strong confinements, the energy barriers for nucleation of new phases are so small that at the standard conditions of adsorption experiments the metastable states are short lived and both the condensation and the desorption occur near equilibrium.

Second, the classical picture of hysteresis in ink-bottle pores implies that the desorption process is controlled exclusively by the diameter of the pore neck. We have shown that the pore blocking effect takes place only when the neck diameter is greater than a certain characteristic size (ca. 4 nm for nitrogen).²¹ Desorption from a cavity fitted with narrower necks occurs at the conditions of cavitation of the metastable stretched fluid and does not appear to depend on the neck diameter. The pressure of cavitation, p_{cav} , is determined by the onset of nucleation at given experimental conditions and may appreciably exceed the liquidlike spinodal pressure, p_{sl} (Figure 1). In this case, the whole adsorption–desorption cycle in the cavity is controlled by its geometry, and the isotherm would be unchanged even if all the necks were closed yet still permeable to vapor. Probably, the absence of pore blocking effects was observed in molecular simulations^{14,15a} at these particular conditions. In the further discussion, the mechanism in which the desorption is controlled by the size of pore necks is referred to as the *pore blocking controlled desorption*, in accord with the conventional picture of pore blocking effects. The desorption mechanism of spontaneous evaporation of the stretched metastable liquid is referred to as *cavitation*. Starting from the original idea put forward by Schofield²³ and elaborated in the works of Kadlec and Dubinin²⁴ and Burgess and Everett,²⁵ the latter mechanism was discussed in the literature based on the limiting tensile strength hypothesis to explain the lower closure point of adsorption hysteresis loops, which is known to be insensitive to the nature of the adsorbent. For sorption of nitrogen at 77.4 K, it is well documented that the lower closure point of adsorption hysteresis varies in a narrow range of relative pressures, from ~ 0.42 to ~ 0.5 .⁵

In this paper we present an elaborated picture of possible pathways of adsorption hysteresis in ink-bottle type pores along with the experimental evidence for three different mechanisms of evaporation, (Figure 1). These mechanisms are: (i) desorption caused by cavitation of the metastable adsorbate, (ii) pore blocking controlled desorption, and also, for the first time, (iii) near-equilibrium desorption in the region of hysteresis from the cavities that have

immediate access to the vapor phase and thus are effectively unblocked. We show that the temperature decrease may lead to transition from the cavitation to the pore blocking regime of desorption. This observation opens up an opportunity to tune the experimental conditions in order to characterize the pore neck size distribution.

2. Experimental Results

The isotherms of capillary condensation and desorption were measured using Autosorb-1C volumetric instrument (Quantachrome) on well-characterized samples of ordered nanoporous materials with cagelike pore structures. Nitrogen and argon isotherms at 77.4 and 87.4 K were measured on a sample of FDU-1.^{18a,18b} FDU-1 possesses a regular periodic structure with cagelike pores of ~ 15 nm in diameter, as calculated by the NLDFT method.²¹ The argon isotherm at 77.4 K and krypton isotherm at 87.4 K were measured on a sample of SBA-16 silica^{20c} (~ 8.5 nm cagelike pores by the NLDFT method). SBA-16 has an ordered *Im3m* structure recently confirmed by electron crystallography.^{20b} FDU-1 and SBA-16 represent the best currently available examples of ordered ink-bottle pore systems.

Figures 2a–c show adsorption isotherms of N₂ and Ar on FDU-1. Repeated measurements are denoted by different symbols. High stability of the material was confirmed by the repeated adsorption measurements performed after the sample was stored at ambient conditions for a period of two years. No change in the isotherm was detected except for the $\sim 6\%$ reduction in the pore volume and surface area due to aging. Ar isotherms at 77 K are plotted using the saturation pressure of the supercooled liquid Ar (~ 230 Torr) rather than the experimentally observed saturation pressure of bulk solid Ar (~ 205 Torr). This choice of the saturation pressure gives a consistent comparison between the Ar isotherms at 77 and at 87 K and was shown to give consistent results when the experimental data at 77 K are compared with the simulated and NLDFT isotherms.²⁶

For all three experimental conditions, the adsorption isotherms exhibit the following characteristic features (see Figure 2). The initial portion of the isotherm corresponds to adsorption in micropores and formation of a poly-molecular film on the pore walls. FDU-1 contains intrawall micropores (their amount N_{lw} is shown in Figure 2a) that are typical for the materials prepared using polymeric surfactants.^{27,28} The sharp capillary condensation step between points A and B indicates a relatively narrow pore size distribution. At point B all mesopores are filled and the uptake at higher pressures corresponds to adsorption in macropores, presumably spaces between particles.

Desorption is considerably delayed and essentially does not occur until the point F (for N₂ at 77 K and Ar at 87 K) or point E (for Ar at 77 K). N₂ and Ar isotherms at 87 K behave alike and exhibit a sharp evaporation step FG at the relative pressures of ~ 0.5 and ~ 0.44 , respectively. However, starting from point E, the Ar isotherm at 77 K is qualitatively different from the others. It exhibits a two-stage evaporation regime: a sharp step FG is preceded by a more gradual part EF.

An important feature of the desorption branches is the presence of a small substep CD, which is more clearly seen on Ar isotherms. This substep transforms into a well-

(26) Neimark, A. V.; Ravikovitch, P. I.; Grun, M.; Schuth, F.; Unger, K. K. *J. Colloid Interface Sci.* **1998**, *207*, 159.

(27) Kruk, M.; Jaroniec, M.; Ko, C. H.; Ryoo, R. *Chem. Mater.* **2000**, *12*, 1961.

(28) Ravikovitch, P. I.; Neimark, A. V. *J. Phys. Chem. B* **2001**, *105*, 6817.

(23) Schofield, R. K. *Discuss. Faraday Soc.* **1948**, *3*, 105.

(24) Kadlec, O.; Dubinin, M. M. *J. Coll. Interface Sci.* **1969**, *31*, 479.

(25) Burgess, C. G. V.; Everett, D. H. *J. Colloid Interface Sci.* **1970**, *33*, 611.

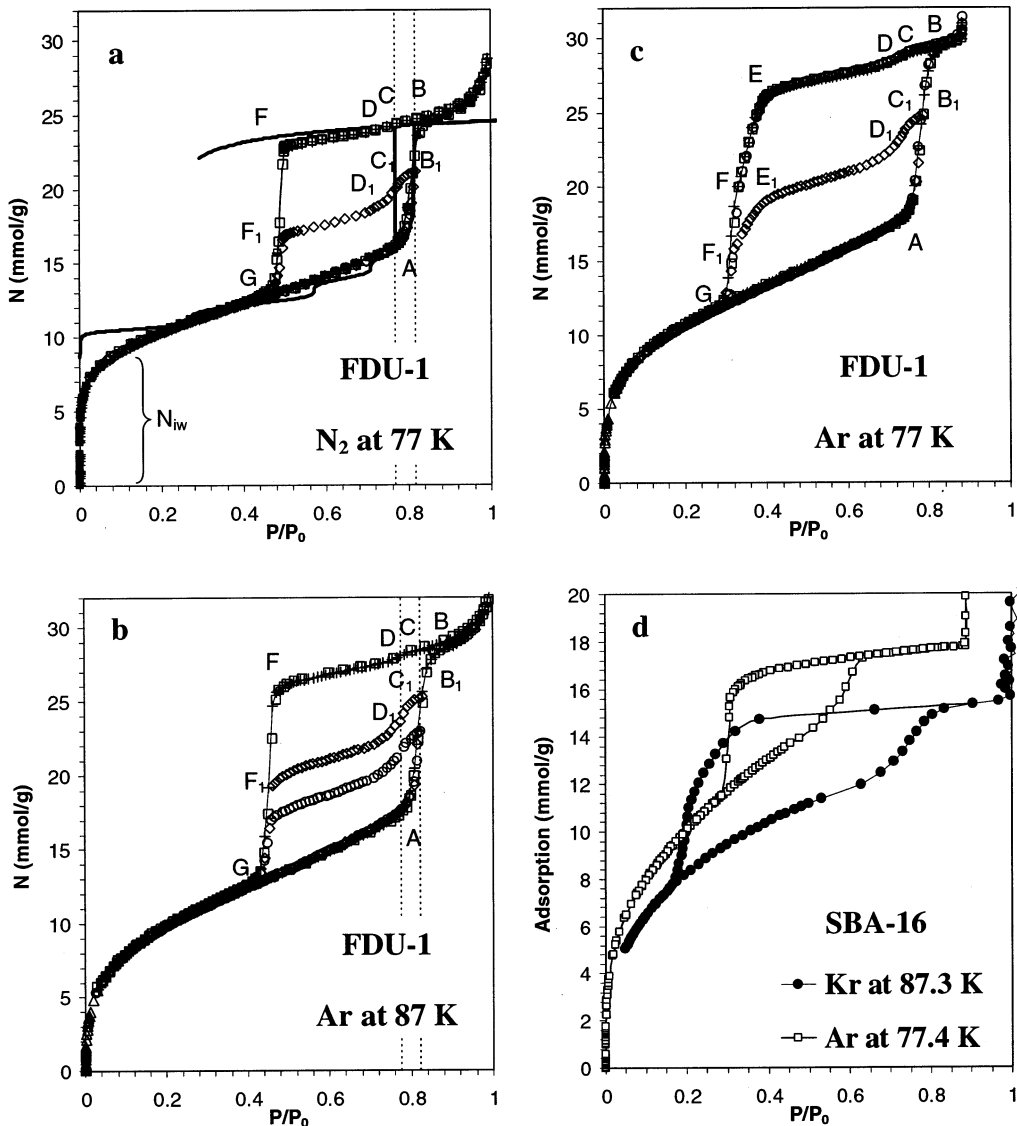


Figure 2. Adsorption isotherms on FDU-1 silica: (a) N_2 at 77.4 K, thick solid line denotes NLDFT isotherm in 15.5 nm spherical pore shifted upward by N_{iw} to account for adsorption in intrawall pores; (b) Ar at 87.3 K; (c) Ar at 77.4 K; (d) adsorption isotherms on SBA-16 [Ar at 77.4 K (open squares) and Kr at 87.3 K (solid circles)] plotted using the saturation pressures of the bulk solid Kr. For (a) and (b), vertical dotted lines indicate positions of the equilibrium (left) and adsorption spinodal transitions (right). Symbols denote different experiments.

pronounced step displayed on scanning desorption isotherms, thus indicating a distinctive mechanism of desorption which will be discussed in detail below. The scanning desorption isotherms were measured starting from the partially saturated sample (indicated as point B_1 for one of the scanning curves; the others are similar). The position of the first step C_1D_1 on the scanning desorption curves $B_1C_1D_1F_1G$ ($B_1C_1D_1E_1F_1G$ for Ar at 77 K) coincides with the position of the substep CD on the main desorption branch. As the pressure is reduced further, the scanning isotherms repeat all the features of the main desorption curves, namely the region of gradual desorption is followed by the one-stage evaporation F_1G for N_2 and Ar at 87 K, and the two-stage evaporation for Ar at 77 K (with steps, E_1F_1 and F_1G).

Figure 2d presents Ar and Kr adsorption–desorption isotherms on SBA-16 silica. The Ar isotherm at 77 K exhibits a single evaporation step, much like N_2 and Ar (87 K) isotherms on FDU-1. However, the Kr isotherm on SBA-16 at 87 K exhibits a two-stage evaporation similar to the Ar isotherm on FDU-1 at 77 K. The substep on the main desorption branch has not been detected for SBA-16.

3. Discussion

We observe several new features of adsorption–desorption hysteresis loops, which are well-defined in ordered cage-like structures and are smeared out in disordered materials: (1) there is a substep on the initial plateau region of the main desorption branch; (2) the scanning desorption isotherms have two distinct steps and are qualitatively different from the smooth scanning curves reported earlier for H1 and H2 type hysteresis loops;^{4,5} (3) as the temperature decreases from 87 K to 77 K, the abrupt step on the desorption isotherm of Ar is split into two steps. These characteristic features of adsorption–desorption isotherms can be explained on the basis of the nonlocal density functional theory NLDFT of capillary condensation.²¹

The comparison of the experimental isotherm with the model NLDFT isotherm calculated for a spherical cavity of 15.5 nm in diameter (Figure 2a) shows that the capillary condensation proceeds in accord with theoretical predictions. The calculated NLDFT isotherm, which was shifted upward by N_{iw} to account for adsorption in intrawall pores ($\sim 0.3 \text{ cm}^3/\text{g}$) is in good agreement with the experimental

data. As it is generally accepted for such wide mesopores, the polymolecular adsorption film becomes metastable^{6,7,29} and condensation is thus delayed until the free energy barrier for nucleation of the liquidlike phase is overcome by fluctuations.²² The capillary condensation occurs practically at the limit of stability of polymolecular adsorption film (vaporlike spinodal point) predicted theoretically,^{21,30–31} where the energy barrier for nucleation vanishes.²² Thus, the step AB (Figures 2a–c) corresponds to the near-spinodal condensation. Using NLDFT adsorption isotherms in spherical pores, we calculated the size distribution of mesopores by the method described earlier.²¹ The distribution was centered at 15 nm with the standard deviation of ~1 nm. Both for N₂ and Ar in 15.5 nm spherical pore, the calculated relative pressure of the thermodynamic equilibrium between the vaporlike and liquidlike phases (vertical dotted lines in Figures 2a and 2b) matches closely the position of the substep CD on the main desorption isotherm and the step C₁D₁ on the scanning desorption isotherms (NLDFT calculations for Ar were performed with the parameters reported earlier for siliceous materials of MCM-41 type²⁶). We therefore conjecture that the steps CD and C₁D₁ correspond to the equilibrium evaporation from the cavities.

Until recently, the possibility that the liquid condensed in spheroidal cavities may evaporate at the equilibrium conditions has not been discussed in the literature. In the classical description of adsorption in ink-bottle pores⁶ it has been explicitly assumed that the evaporation is controlled by the size of the pore necks. As related to the equilibrium desorption, the authors assumed that “there is no means of establishing an equilibrium path of desorption in the case of spheroidal cavities”.⁶ As was noted in the Introduction, in the preceding paper²¹ we have shown that in highly ordered materials with sufficiently small cagelike pores (~3–6 nm in diameter) the reversible capillary condensation step corresponds to the equilibrium transition, as calculated by the NLDFT for spherical pores. The validity of this interpretation has been confirmed by the fact that the pore diameters predicted by NLDFT were in excellent agreement with the pore sizes obtained from geometrical models of these structures.²¹ In sufficiently narrow pores the free energy barrier for nucleation is relatively low while the fluctuations are strong, which leads to the regime of reversible capillary condensation/evaporation.³²

Wider spherical pores can also exhibit near-equilibrium evaporation. In the blocked cavities larger than ~6 nm, the barrier for the liquid–vapor nucleation (bubble formation) is very high. Therefore, desorption does not occur until either the liquid evaporates from the neighboring pores, which block access to the vapor phase (classical pore blocking effect), or spontaneous cavitation of the metastable liquid trapped in the cavity occurs (see possible scenarios in Figure 3). The equilibrium evaporation, however, can occur when the cavity has a direct contact with the vapor phase, so that the liquid–gas interface can be formed, and thus the cavity is effectively unblocked. This can happen when the cavity has a short neck or a wide window opening. We conjecture that the substep CD corresponds to the evaporation from unblocked

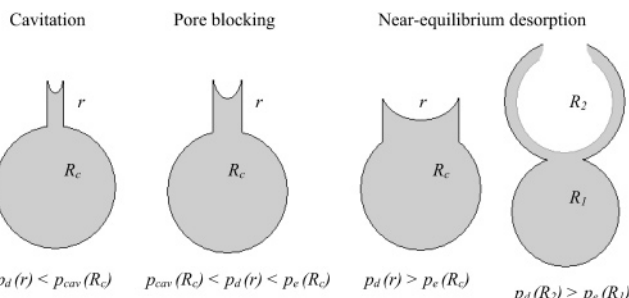


Figure 3. Schematic illustration of three different desorption mechanisms from ink-bottle type pores (see text).

cavities which have immediate access to the outer surface of the primary particles of FDU-1. The number of such cavities is small, and thus we observe just a small substep on the desorption branch. When the particle is partially saturated, as in the case of the scanning desorption curves, a larger number of cavities remains unblocked and has direct access to the vapor phase. Evaporation from these pores gives rise to the step C₁D₁ on the scanning desorption curves. The simplest situation of two adjacent overlapping cavities of slightly different sizes ($R_2 > R_1$) is shown in Figure 3. In this case the cavity R_1 is filled while the cavity R_2 has only a polymolecular adsorption film on its interior surface. Upon decrease in pressure, the cavity R_1 will empty at the pressure that is close to the equilibrium conditions for a spherical pore of radius R_1 .

Once all cavities that have access to the vapor phase empty, the desorption transits into the plateau region, which corresponds to the evaporation from the polymolecular films in the emptied pores and to the reduction of density of condensed liquid in the blocked cavities. From the scanning isotherm we can determine the fraction of cavities that were blocked in the beginning of desorption at point B₁ and remained filled after the evaporation from unblocked pores had occurred. Indeed, in the plateau region, the scanning isotherm is determined by the fraction of filled cavities, α , and is given by

$$N_{\text{scan}} = (1 - \alpha)N_{\text{ads}} + \alpha N_{\text{des}}$$

In Figure 4, we demonstrate the validity of this relation for the scanning isotherm of Ar at 87 K. The fractions of filled pores were determined from the best fit to experimental data in the region indicated by arrows.

Evaporation from the blocked pores along the main and scanning desorption isotherms occurs abruptly at the same pressure, which lies between the equilibrium pressure, p_e , and the liquidlike spinodal pressure, p_{sl} (Figure 2). While in the classical models of independent ink-bottled pores^{1,2,6} and percolation models of pore networks,^{11–13} the onset of evaporation from the blocked pores is assumed to be controlled entirely by the sizes of pore necks, in the case of FDU-1 we observe spontaneous cavitation, which occurs upon achievement of the conditions of instability of condensed liquid. The cavitation pressure, p_{cav} , is determined by the nucleation conditions and may exceed the liquidlike spinodal pressure, p_{sl} (Figure 1). Abrupt desorption steps at the same relative pressure ($p_{cav}/p_0 \sim 0.5$ for N₂ at 77 K) were observed for other cagelike structures with different pore sizes.^{18,20a} A similar behavior was recently reported for materials consisting of open and blocked cylindrical pores.^{17d} The spontaneous desorption occurs in the cavities with the necks narrower than the neck from which the evaporation occurs at the pressure of cavitation p_{cav}/p_0 . The limiting size of necks that cannot be opened at pressures larger than the pressure of

(29) Saam, W. F.; Cole, M. W. *Phys. Rev. B* **1975**, *11*, 1088.

(30) Neimark, A. V.; Ravikovich, P. I.; Vishnyakov, A. *Phys. Rev. E* **2000**, *62*, R1493.

(31) Neimark, A. V.; Ravikovich, P. I. *Microporous Mesoporous Mater.* **2001**, *44–45*, 697.

(32) Ravikovich, P. I.; Domhnaill, S. C. Ó.; Neimark, A. V.; Schüth, F.; Unger K. K. *Langmuir* **1995**, *11*, 4765.

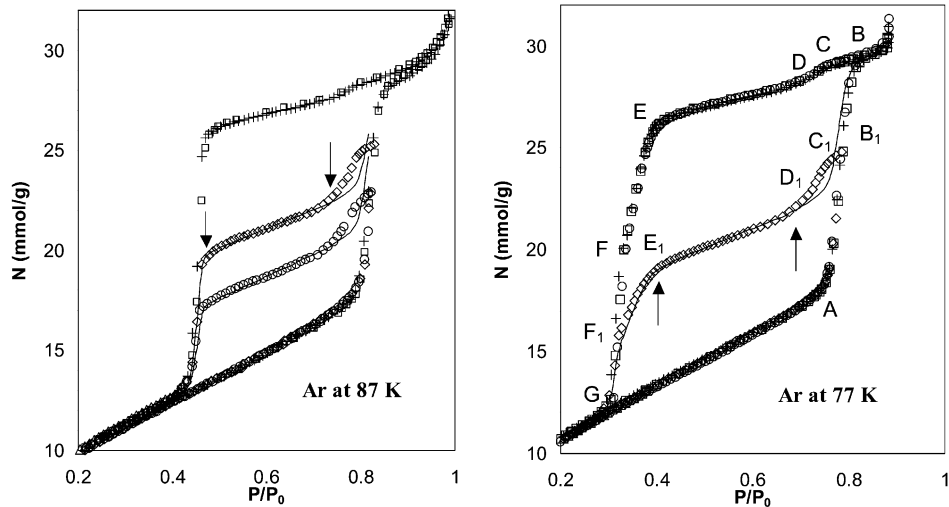


Figure 4. Fit of Ar scanning desorption isotherms on FDU-1 at 87 and 77 K (lines) in the pressure interval indicated by arrows. At 87 K the fraction of blocked pores on the upper and lower scanning curves is 0.52 and 0.32, respectively. At 77 K, the fraction of blocked pores is 0.44.

cavitation p_{cav}/p_0 are estimated by the NLDFT model for the infinitely long cylindrical pores as ~ 5 nm for N_2 at 77 K and for Ar at 87 K, and ~ 4 nm for Ar at 77 K. Since the neck sizes in the FDU-1 sample were smaller than 5 nm, the desorption of N_2 at 77 K and Ar at 87 K occurred in the regime of cavitation.

Figures 1 and 3 summarize three possible evaporation regimes from ink-bottle type pores. The conditions at which one or the other mechanism is operative depend on the pressure p_d at which the neighboring pores empty (note that the pore neck itself is considered as the neighboring pore). Each cavity is characterized by two characteristic pressures—the pressure of equilibrium transition, p_e , and the pressure of spontaneous cavitation, p_{cav} . When the neighboring pores empty at the pressure lower than p_{cav} , evaporation occurs via cavitation. When the neighboring pores empty at the intermediate pressure, between p_{cav} and the equilibrium pressure p_e , we deal with the classical pore blocking effect and such a cavity-neck assembly can be truly called an ink-bottle pore. When the neighboring pores empty at the pressure that exceeds p_e , the cavity becomes effectively unblocked and will empty at the equilibrium pressure. Two possible examples, a cavity with a wide cylindrical neck and slightly overlapping spherical pores, are shown in Figure 3.

To elucidate the two-stage behavior of the desorption isotherm of Ar at 77 K, one can compare this isotherm (Figure 2c) with the Ar isotherm on a sample of SBA-16 material^{20c} (Figure 2d), which contains ~ 8.5 nm wide cavities with the standard deviation of ~ 0.5 nm, connected by necks < 4 nm. If the desorption from SBA-16 were controlled by the size of necks, the pressure of desorption would be lower than 0.3 ($p/p_0 = 0.3$ corresponds to the desorption of Ar at 77 K from a cylindrical channel of 4 nm in diameter²⁶). Thus, the second sharp step FG on the desorption isotherm of Ar at 77 K on FDU-1 material is interpreted as cavitation in pores blocked by the necks smaller than ~ 4 nm. The preceding step EF corresponds to the desorption from cavities blocked by wider necks from ~ 4 nm to ~ 5 nm in diameter. Note that the neck sizes may be in reality somewhat smaller than these values estimated from the NLDFT model for infinitely long cylinders, since the condensation transitions in finite length pores shift to higher relative pressures compared to the infinitely long pores.

The transition from the one-stage (N_2 at 77 K, Ar at 87 K) to two-stage desorption (Ar at 77 K) can be explained

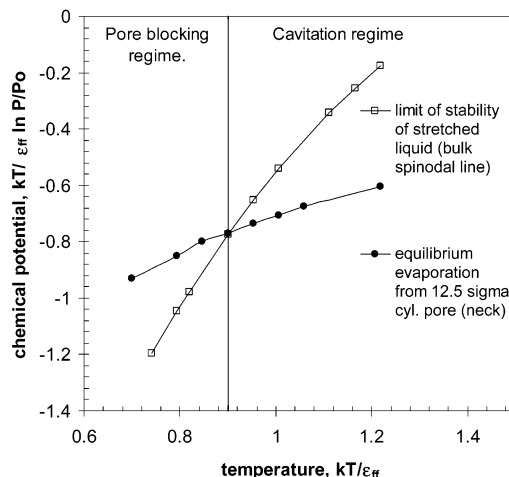


Figure 5. Schematic illustration of the temperature dependence of the hysteresis loop in sufficiently large (> 6 –7 nm) ink-bottle pores with ~ 4 nm neck (N_2 at 77 K). NLDFT bulk spinodal line estimates the limit of stability of the stretched metastable liquid. The line of equilibrium evaporation from 12.5 σ_0 cylindrical pore approximately describes evaporation from the pore neck.

by the different temperature dependencies of the conditions of cavitation and the conditions of evaporation from necks. The temperature dependencies of the chemical potentials of cavitation and evaporation are shown in Figure 5, which illustrates schematically two different mechanisms of evaporation from a large ink-bottle type pore. The NLDFT calculations were performed for N_2 . The chemical potential of cavitation was estimated from the spinodal of bulk liquid. The equilibrium chemical potential in the ~ 4 nm infinitely long cylindrical pore was used to approximate the conditions of evaporation from the neck. Two scenarios of the process of desorption can be suggested as the chemical potential decreases from zero (saturation). At a relatively high (but subcritical) temperature, the liquid condensed in the cavity becomes unstable and evaporates before the conditions for the equilibrium evaporation from the necks are met. This cavitation regime is observed for N_2 at 77 K and Ar at 87 K on FDU-1 and Ar at 77 K on SBA-16. Note that the pressure of cavitation does not appear to depend significantly on the size of cavities at a given temperature; the cavity diameter itself is irrelevant as long as it is sufficiently larger than the

pore neck. Below the crossover temperature, which depends on the neck size, evaporation from the cavity occurs after the pore neck opens. Thus, the portions EF and E₁F₁ of Ar isotherms at 77 K (Figure 2c) correspond to the desorption controlled by pore blocking. The slope of these portions reflects the size distribution of necks (from ~ 5 nm and below) and the pore network connectivity. Due to the distribution of pore necks below ~ 4 nm, the desorption process is not fully completed upon the achievement of the conditions of cavitation at points F and F₁ (which corresponds to the crossover point in Figure 5) and further decreases in the chemical potential leads to spontaneous evaporation reflected by sharp steps FG and F₁G.

A decrease of the pore neck diameter has an effect similar to an increase of the temperature: it leads to the transition from the pore blocking to the cavitation regime of evaporation. Thus, to characterize the neck size distribution, the temperature should be chosen low enough to provide the pore blocking regime of desorption. For Kr at 87 K, which is below its bulk triple point by 28.5 K, we still are able to observe the pore filling of SBA-16 (Figure 2d). On the desorption path, one can see a transition from the gradual pore blocking regime of desorption to the abrupt, spontaneous evaporation, which is qualitatively similar to that observed for Ar on FDU-1 at 77 K. Note that for SBA-16 we do not observe the substep related to the evaporation from the unblocked pores facing the outer surface of particles. This is probably due to the larger size of the primary particles in SBA-16, which makes this amount too small to be detected.

It should be noted that Ar at 77.4 K and Kr at 87.3 K are below their bulk triple points by 6.5 and 28.5 K, respectively. Generally, solidification/melting transition for a fluid confined in silica pores is suppressed.^{33–35} In particular, Ar at 77 K behaves as a liquid in $\sim 3\text{--}5$ nm cylindrical pores of MCM-41, and condensation/evaporation pressures are predicted rather accurately by the NLDFT, provided that the experimental pressures are reduced by the saturation pressure of the supercooled liquid Ar.^{26,36} What is remarkable is that the condensation and evaporation behavior for Ar at 77 K in ~ 15 nm pores of FDU-1 and, especially, Kr at 87 K in ~ 8.5 nm SBA-16 is similar to that for fluids above the triple point. In particular, when the experimental condensation and equilibrium pressures of Ar in FDU-1 are reduced by the saturation pressure of supercooled liquid Ar,²⁶ the results are in agreement with the NLDFT calculations in spherical pores. However, we cannot totally exclude the possibility of solidification of Ar in FDU-1 or Kr in SBA-16 because the pores in these materials are larger than in MCM-41. Adsorption behavior of Ar in FDU-1 is consistent with the studies of Ar sorption both above and below the triple point in ~ 10 nm (cylindrical model) Vycor and Gelsil glasses,³⁵ which exhibit a capillary condensation/solidification step at about the same pressure. These studies concluded that the solid Ar condensate undergoes a first-order transition very much like the liquid.³⁵ It should also be noted that below the triple point there exists an upper

(33) (a) Warnock, J.; Awschalom, D. D.; Shafer, M. W. *Phys. Rev. Lett.* **1986**, 57, 1752. (b) Molz, E.; Wong, A. P. Y.; Chan, M. H. W.; Beamish, J. R. *Phys. Rev. B* **1993**, 48, 5741.

(34) Gelb, L. D.; Gubbins, K. E.; Radhakrishnan, R.; Sliwinska-Bartkowiak, M. *Rep. Prog. Phys.* **1999**, 62, 1573.

(35) (a) Huber, P.; Knorr, K. *Phys. Rev. B* **1999**, 60, 12657. (b) Wallacher, D.; Knorr, K. *Phys. Rev. B* **2001**, 63, 104202.

(36) Ravikovich, P. I.; Haller, G. L.; Neimark, A. V. *Adv. Colloid Interface Sci.* **1998**, 76–77, 203.

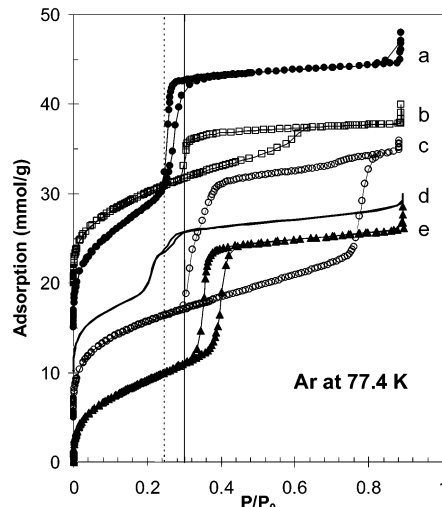


Figure 6. Adsorption isotherms of Ar at 77.4 K on ordered materials with cagelike and cylindrical pores: (a) 3.6 nm cylindrical MCM-41 (black circles); (b) 8.5 nm cages, <4 nm necks SBA-16 (open squares); (c) 15 nm cages, <5 nm necks FDU-1 (open circles); (d) 3–4 nm bimodal cylindrical MCM-41 (solid line); (e) 4.5 nm cylindrical MCM-41 (triangles). The isotherms are shifted by 5 mmol/g. The vertical dashed and solid lines indicate the lower closure point of hysteresis in cylindrical and spherical pore geometries, respectively. The isotherms are plotted using the saturation pressure of the supercooled liquid Ar.

limit of pores in which condensation may occur.³⁷ In particular, we were unable to condense Kr in FDU-1 at 87 K.

Finally, let us make a comment about the relation between the pressure of cavitation and the lower closure point of hysteresis. It is generally believed that the lower closure point of hysteresis is determined by the conditions of cavitation that depend mostly on the adsorbate and the temperature and vary insignificantly from one porous material to another.⁵ Indeed, as noted above, the pressures of the sharp evaporation step in different cagelike structures are almost the same. In Figure 6 we compare Ar adsorption isotherms at 77 K on materials with spherical (SBA-16 and FDU-1) and cylindrical (MCM-41) pores. To give a more complete picture of possible hysteresis behavior, we added the isotherm with type H1 hysteresis loop on reference MCM-41 with 4.5 nm channels.^{32,26} Here, the position of the desorption branch reflects the condition of equilibrium evaporation from open-ended cylindrical channels and is not related to the lower closure point of the hysteresis loop. As the pore size decreases, the hysteresis loops narrow and shift to lower pressures. This is seen for a sample of MCM-41²⁶ with 3.6 nm channels and for a bimodal aluminosilicate, which has two groups of cylindrical channels with slightly different pore diameters.³⁶ The lower closure point of the hysteresis loop for these entirely different samples is almost the same, and what is remarkable is that the corresponding pressure is appreciably lower than that for SBA-16 and FDU-1. The pressure of spontaneous evaporation/cavitation in spherical pores is ~ 0.055 Po higher than the lower closure point of the hysteresis loop in materials with cylindrical pores. We conclude that the lower closure point of the hysteresis loop depends not only on the adsorbate and the temperature but also on the pore geometry. This observation, which questions the conventional assumption,⁵ is in line

(37) (a) Thommes, M.; Köhn, R.; Fröba, M. *J. Phys. Chem. B* **2000**, 104, 7932. (b) Thommes, M.; Köhn, R.; Fröba, M. *Appl. Surf. Sci.* **2002**, 196, 239.

with the NLDFT predictions that the liquidlike spinodal and, therefore, the conditions for cavitation, depend on the pore geometry.

4. Conclusions

We have studied experimentally the adsorption–desorption hysteresis of N₂, Ar, and Kr in 3D porous cagelike structures of FDU-1 and SBA-16 silicas, which currently represent the best available examples of ordered ink-bottle pore systems. Special attention was paid to the analysis of scanning desorption isotherms that exhibited unique features not reported before for other mesoporous materials. These isotherms present the experimental evidence for various mechanisms of evaporation from ink-bottle type pores. These mechanisms are: (i) spontaneous evaporation due to cavitation, (ii) pore blocking controlled desorption, and also, for the first time, (iii) near-equilibrium desorption in the region of hysteresis from the cavities that have immediate access to the vapor phase through the relatively wide openings, and thus are effectively unblocked. The experimental results agree with the density functional theory of capillary condensation hysteresis in spherical cavities.²¹

The onset of desorption from filled cavities is related to the formation of a liquid–vapor interface, which may proceed via different mechanisms. The near-equilibrium desorption, indicated by steps CD and C₁D₁ on the isotherms on FDU-1 (Figures 2a–c), can occur in an unblocked cavity in which an interface/meniscus is formed at the pore opening. The fraction of unblocked cavities in the partially saturated sample can be calculated from the scanning isotherm. Evaporation from a blocked cavity is

controlled by a competition between the formation of menisci after the emptying of the neighboring pores (classical pore blocking effect), and the nucleation of bubbles in the stretched metastable liquid.

We show that the decrease in temperature may lead to the transition from the cavitation of maximum stretched liquid to the pore blocking controlled desorption indicated by the two-stage desorption branches on the isotherms of Ar at 77 K on FDU-1 and Kr at 87 K on SBA-16 (Figures 2c, 2d, 4b). This observation opens up an opportunity to tune the experimental conditions in order to characterize the pore neck size distribution.

The pressure of the spontaneous evaporation from ink-bottle pores was found to be ~0.055 Po higher than the lower closure point of the hysteresis loop in materials with cylindrical pores (Figure 6). Thus, the lower closure point of the hysteresis loop depends on the pore geometry, which questions the conventional assumption⁵ that this point depends entirely on the temperature and physical properties of the adsorbate and is not sensitive to the nature of the porous material. Our observation is in line with the NLDFT and MC simulation predictions that the liquidlike spinodal, and therefore, the conditions for cavitation depend on the pore geometry.

Acknowledgment. We thank Dr. Dongyuan Zhao (Fudan University) and Dr. Pascal Van Der Voort (University of Antwerpen) for providing us with the samples of FDU-1 and SBA-16 materials, respectively. The work was supported by the TRI/Princeton exploratory research program.

LA026140Z